Liquid Structure, Thermodynamics, and Mixing Behavior of Saturated Hydrocarbon Polymers. 1. Cohesive Energy Density and Internal Pressure

Janna K. Maranas

Department of Chemical Engineering, The Pennsylvania State University, University Park, Pennsylvania 16802

Maurizio Mondello and Gary S. Grest

Corporate Research Laboratories, Exxon Research and Engineering Company, Annandale, New Jersey 08801

Sanat K. Kumar

Department of Materials Science and Engineering, The Pennsylvania State University, University Park, Pennsylvania 16802

Pablo G. Debenedetti and William W. Graessley*

Department of Chemical Engineering, Princeton University, Princeton, New Jersey 08544

Received December 2, 1997; Revised Manuscript Received July 6, 1998

ABSTRACT: Thermodynamic properties related to the miscibility of saturated hydrocarbon polymers were investigated by simulation methods. Cohesive energy density, Π_{CED}, widely used to estimate the mutual solubilities of ordinary liquids, cannot be measured for polymers, but values of Π_{CED} have been inferred from data on internal pressure, Π_{IP}. Both Π_{CED} and Π_{IP} were obtained in this work by molecular dynamics simulations with a united atom model. The effects of chain microstructure and chain length were examined. The simulation model was tested with data for various heptane isomers (the C7 series), for which Π_{CED} and Π_{IP} are known. It was then applied to oligomers of various polymer species (the C30 series) with known Π_{IP}. Simulation values of Π_{CED} and Π_{IP} were also extrapolated to their long-chain limits in selected cases. The values and trends with structure were generally consistent with the experimental data available for the C7 and polymeric liquids. The ratio $a = \Pi_{CED}/\Pi_{IP}$ was found to decrease from near unity for the C7 series to polymeric values of approximately 0.75. This result agrees remarkably well with $a = 0.72 \pm 0.11$, a range of values that had been inferred from the analysis of interactions in blends of saturated hydrocarbon polymers and PVT data on the pure components. The implication of these results and their relationship to various mixing theories are discussed.

Introduction

Polyolefins are saturated hydrocarbon polymers of considerable commercial importance. Blends of polyolefins are used extensively, and their properties, like those for any blend, depend strongly on the underlying phase relationships. Extensive information has become available recently on the molecular interactions that govern the liquid−liquid-phase behavior of polyolefin blends.[1,2] These data were obtained, for the most part, by small-angle neutron scattering (SANS) measurements on blends of model polyolefins. Results were expressed in terms of the Flory−Huggins model:

$$\Delta g_m = RT\left[\frac{\phi_i \ln \phi_i}{V_i} + \frac{\phi_j \ln \phi_j}{V_j}\right] + X_{ij}(T)\phi_i\phi_j \qquad (1)$$

in which Δg_m is the Gibbs free energy of mixing per unit volume, V_i and V_j are the molar volumes of components i and j, respectively, ϕ_i and ϕ_j are their volume fractions in the mixture ($\phi_i = 1 - \phi_j$), and $X_{ij}(T)$ is the interaction density coefficient for the pair.[2]

The SANS-based values of X_{ij} were obtained over a range of temperatures, typically 25−167 °C, for numerous pairs of polyolefin species. A large number of the pairs were found to mix in a regular fashion, by which we mean that the observed values of the interaction coefficients were consistent with a solubility parameter formalism.[3] Thus,

$$X_{ij}(T) = [\delta_i(T) - \delta_j(T)]^2 \qquad (2)$$

in which $\delta_i(T)$ and $\delta_j(T)$ are, nominally, the solubility parameters of species i and j. The values of these parameters, all relative to those for some arbitrary reference species, were assigned on the basis of internal consistency tests of $X_{ij}(T)$ for blends with common components. The procedures are described in detail elsewhere.[4] The result is a catalog of values of $[\delta_i(T) - \delta_{ref}(T)]_{SANS}$ that predicts, within the errors, the values of $X_{ij}(T)$ for about 80% of the blends investigated.

The present work addresses the microscopic origins of interactions in mixtures of saturated hydrocarbon polymers. Various proposals have been made recently about the relative importance of entropic and enthalpic contributions. Bates et al.[5,6] have suggested that a mismatch in the component persistence lengths gives rise to a repulsive interaction that is primarily entropic in nature. Schweizer et al.[7,8] have inferred a connection between the interactions and packing at the monomeric level. Thus, a large body of their PRISM-based work[9−12] suggests a strong coupling between local packing and

S0024-9297(97)01755-5 CCC: $15.00
Published on Web 09/12/1998

cohesive energy, leading to a net interaction from differences in chemical microstructure that is primarily enthalpic in nature. Freed et al.[13−15] have applied lattice cluster theory to packing at both the local and persistence-length scales as well as to many other potential sources of interactions. Their work suggests that, depending on the system, almost any combination of enthalpic and entropic contributions can be obtained. The molecular dynamics study described here and in the companion paper[16] attempts to clarify such issues as these.

The solubility parameter is the positive square root of the cohesive energy density:[3]

$$\delta = (\Pi_{CED})^{1/2} \tag{3}$$

For monomeric liquids, the cohesive energy density is simply the internal energy of evaporation per molar volume of liquid:

$$\Pi_{CED} = \frac{U_G - U_L}{V_L} \tag{4}$$

A different expression is appropriate for polymeric liquids (see below), but in any case, Π_{CED}, an easily measured quantity for ordinary liquids, is not measurable at all for polymeric liquids. Some indirect evidence from data on the internal pressure of the liquid, obtainable by PVT measurements and equal to Π_{CED} for van der Waals liquids,[3]

$$\Pi_{IP} \equiv \left(\frac{\partial U_L}{\partial V}\right)_{T,N} \tag{5}$$

suggests that the values of $[\delta_i(T) - \delta_{ref}(T)]_{SANS}$ do, indeed, reflect the underlying cohesive energy densities of the various species.[1] Other interpretations are possible, however, as noted above, and for basic understanding and purposes of generalization, such uncertainty is undesirable. A second area of uncertainty is the origin of the irregular mixing found in the 20% of blends that do not obey eq 2. The sources of mixing irregularity are unknown. There are no obvious trends in irregularity with the component chemical structures, although there are some indications of a correlation with the PVT measurements used to obtain Π_{IP}.[1]

Both these areas of concern involve microscopic and experimentally unobservable aspects of the interactions. The molecular dynamics simulations described here are an attempt to address them as directly as possible. The relationship between cohesive energy density and internal pressure for saturated hydrocarbons, including the evolution of both Π_{IP} and Π_{CED} with increasing chain length, is examined in this paper. The trends with chemical microstructure are also compared with those found in the experimental values of Π_{IP} and $[\delta_i(T) - \delta_{ref}(T)]_{SANS}$. The companion paper[16] explores the microscopic aspects of regular and irregular mixing through the intermolecular pair distribution functions of the individual components.

The simulations focus on seven species—polyethylene (PE), polypropylene (PP), head-to-head polypropylene (hhPP), poly(1-butene) (PB), polyisobutylene (PIB), poly(ethylene-*alt*-propylene) (PEP), and poly(ethylene-*alt*-1-butene) (PEB). Their skeletal repeating structures are shown in Figure 1. Blends involving these species

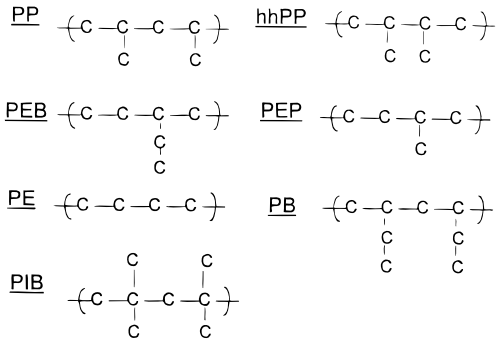

Figure 1. Repeating unit architectures of the C30 series and polymeric species. The hydrogens are omitted for clarity.

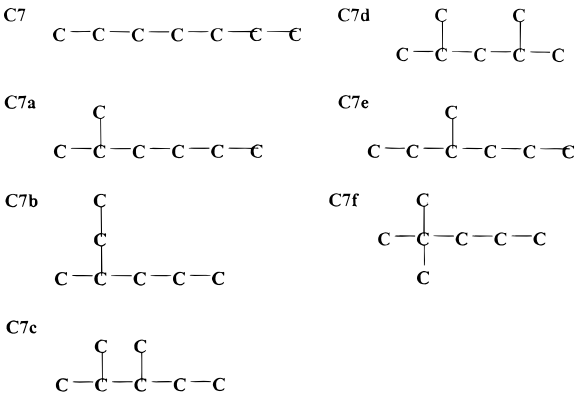

Figure 2. Molecular architectures of the C7 series. The hydrogens are omitted for clarity.

had been studied extensively in the earlier SANS work.[1,2] Owing to the synthesis method, some of the polymers contained small amounts of saturated hydrocarbon co-units, the largest being ~7% for both PEB and PEP.[17] Separate studies showed the co-unit effects at this level to be small but still detectable. Simulations for PEB and PEP were conducted with the co-units included in their structures to make the comparisons with experiment as direct as possible. Oligomers of the seven species (the C30 series) were simulated, and the chain length dependence was investigated for three of them (PE, PP, and hhPP). The effect of tacticity was explored with the PP and hhPP structures. Only the isotactic versions of PEP, PEB, and PB were tested. The model was tested by simulating several isomers of heptane (the C7 series) with known values of both Π_{CED} and Π_{IP}.[18] Their skeletal structures are shown in Figure 2.

The Simulation Model

The model is an extension of the optimized force field for liquid hydrocarbons (OPLS) introduced by Jorgensen et al.[19] The united atom method is used, where interactions between C, CH, CH_2, and CH_3 groups, rather than between individual carbon and hydrogen atoms, are considered. As in ref 19, distinctions are made between methyl groups attached to secondary, tertiary, and quartenary carbons. Nearest-neighbor intramolecular interactions are represented by constraint forces that maintain the separation distance at 1.54 Å. The bending potential takes the form

$$u_{ij}^{b} = \frac{k_b}{2}(\theta_{ij} - \theta_b)^2 \tag{6}$$

in which θ_b is the equilibrium angle, and θ_{ij} is the angle between successive bonds. An ad hoc harmonic potential,

Table 1. Bonded Interaction Parameters

parameter[a]	value
bond length	1.54 Å
bending constant, k_b	124.18 kcal/(mol rad^2)
equilibrium bending angle, θ_b[b]	114°
sp_3 inversion constant	80.0 kcal/(mol rad^2)
equilibrium sp_3 inversion angle	27.25°
torsion constants (X−CH_2−CH_2−Y)	
a_0	2.007 kcal/mol
a_1	4.012 kcal/mol
a_2	0.271 kcal/mol
a_3	−6.290 kcal/mol
torsion constants (X−CH−CH−Y)	
a_0	0.292 kcal/mol
a_1	1.128 kcal/mol
a_2	0.670 kcal/mol
a_3	−2.840 kcal/mol
torsion constants (X−CH−CH_2−Y or X−CH_2−CH−Y)	
a_0	0.814 kcal/mol
a_1	1.792 kcal/mol
a_2	0.389 kcal/mol
a_3	−3.673 kcal/mol
torsion constants (X−C−CH_2−Y or X−CH_2−C−Y)	
a_0	0.567 kcal/mol
a_1	1.700 kcal/mol
a_2	0.000 kcal/mol
a_3	−2.267 kcal/mol

[a] All parameters except the X−C−CH_2−Y and X−CH−CH−Y torsional constants were adapted from ref 19. [b] For PIB, the C−CH_2−C bending angle θ_b was taken to be 122°, and perfect tetrahedral orientation of bonds around quaternary carbons was assumed.[20,21]

Table 2. Nonbonded Interaction Parameters

pair[a]	σ_{ij} (Å)	ϵ_{ij} (kcal/mol)
C−X	3.800	0.050
CH−X	3.850	0.080
CH_2−X	3.905	0.118
CH_3−CH_3	3.775	0.207
CH_2−CH_3	3.905	0.175
CH−CH_3	3.910	0.160
C−CH_3	3.960	0.145

[a] X indicates any united atom; all values were taken from ref 19.

similar to the bending term, is introduced to prevent umbrella inversion of the sp_3 bond configuration at tertiary carbon branch points. The torsional interaction is expressed as a polynomial in the cosine of the torsional angle, ω_{ij}:

$$u_{ij}^{\ t} = \sum_k a_k[\cos(\omega_{ij})]^k \tag{7}$$

The parameters for bonded interactions are given in Table 1. For simulation of PIB, the torsional potentials of Boyd and Krishna Pant[20,21] have been adopted.

The nonbonded forces are characterized by Lennard-Jones (LJ) interaction sites located at the position of each carbon center of mass. The LJ potential has the form

$$u_{ij}^{\ L,J} = 4\epsilon_{ij}\left[\left(\frac{\sigma_{ij}}{r_{ij}}\right)^{12} - \left(\frac{\sigma_{ij}}{r_{ij}}\right)^{6}\right] \tag{8}$$

Both intermolecular and intramolecular nonbonded interactions are allowed, provided the sites are not connected by fewer than four bonds. (If connected by three or fewer bonds, they interact through one of the bonded interaction terms.) The nonbonded potential parameters are given in Table 2.

All simulations were conducted in the (N,V,T) ensemble with a system of 50 molecules. At the densities investigated, this system size allows calculation of the pair distribution function out to approximately 18 Å, well past arrival at the $g(r) = 1$ plateau. An increase in size to 100 and 200 molecules was found to have a negligible effect on the cohesive energy density values.[22] A temperature of 150 °C was used in all simulations except those for the C7 series, which were conducted at 20 °C. The simulation volumes were based on the experimental polymeric densities at 0.1 MPa and 150 °C. Since united atom potentials do not give reliable densities, we did not use constant pressure simulations to estimate the density. Oligomeric densities are experimentally known only for PE.[23] For the other species, the C30 density at 150 °C was calculated with the polymeric density and the PE oligomer/polymer density ratio at 150 °C:

$$\rho_{C30}^{i} = \rho_{polymer}^{i}\left(\frac{\rho_{C30}^{PE}}{\rho_{polymer}^{PE}}\right) \tag{9}$$

Table 3. Simulation Input Data for the C30 Series

material	density (g/cm^3) at 150 °C	united atoms per oligomer
PE	0.7276	30
hhPP	0.7454	31
PP	0.7306	31
PB	0.7510	31
PEP	0.7313	31
PEB	0.7443	31
PIB	0.8012	33

The resulting C30 densities are given in Table 3, along with the actual number of united atoms used per molecule in each case, the latter chosen to give integer numbers of repeat units in each case. The known densities of the C7 series at 20 °C were used.

A constant temperature was maintained during each simulation using the velocity rescaling algorithm of Berendsen et al.[24] The equations of motion were integrated by means of the standard velocity Verlet algorithm,[25] and the bond length was kept constant using the RATTLE algorithm.[25]

The cohesive energy density, as expressed by eq 4, is modified for polymers in order to reflect only the intermolecular part of the energy. Thus, we used

$$U_L - U_G = U_{inter} \tag{10}$$

Accordingly, the cohesive energy density is the average of the (negative) intermolecular potential energy, $-\bar{\Psi}_{inter}$, divided by the simulation volume. The evaluation of internal pressure was based on its definition (eq 5). Thus, the average of total potential energy, $-\bar{\Psi}_{total}$, was determined for several simulation densities near the density of interest, and internal pressure was obtained as the slope of U vs V at that density. (From equipartition, the average kinetic energy is independent of volume and so was omitted.) The pair distribution function was also obtained by implementing its definition.[26] Thus, relative to one united atom, the average number of united atoms from all molecules except its own, located at r in the volume element $4\pi r^2\,dr$, was evaluated, and the results were then averaged over all united atoms and finally normalized to unity at large distances to obtain the intermolecular pair distribution $[g(r)]_{inter}$. If the first average is over all other united atoms, the result is the total pair distribution $[g(r)]_{total}$, a property that can be compared with elastic scattering data.[26] Both distributions were collected for discussion in the companion to this paper.[16]

A time step of 5 fs was used in all simulations. After an initial 150-ps equilibration, the cohesive energy data were collected over 250-ps intervals. Tracking Π_{CED} as a function of time step revealed little change after 20 ps.[22] Data for the pair distributions were collected over 500-ps intervals. Comparisons with results for 900- and 1400-ps intervals showed no further changes.[22]

Internal pressure determinations were made with internal energy data for the largest range of volumes that could be

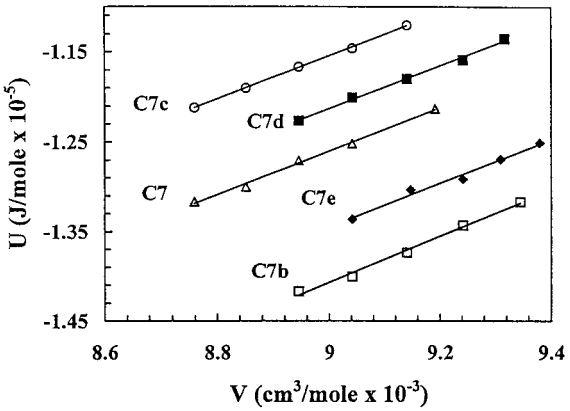

Figure 3. Internal energy as a function of volume for the C7 series. The results for some species have been shifted vertically for clarity.

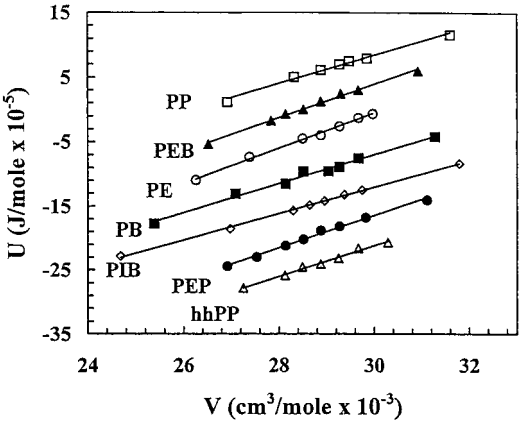

Figure 4. Internal energy as a function of volume for the C30 series. The results for some species have been shifted vertically for clarity.

Table 4. Experimental Data and Simulation Results at 20 °C for the C7 Series

material	density[a] (g/cm^3)	Π_{CED} (MPa) exptl[a]	Π_{CED} (MPa) simul	Π_{IP} (MPa) exptl[a]	Π_{IP} (MPa) simul
C7, *n*-heptane	0.6837	235	247	256	243
C7a, 2-methylhexane	0.6789	221	230	249	
C7b, 3-ethylpentane	0.6984	231	245	267	261
C7c, 2,3-dimethylpentane	0.6952	222	230	259	238
C7d, 2,4-dimethylpentane	0.6745	206	212	236	238
C7e, 3-methylhexane	0.6870	226	237	252	247
C7f, 2,2-dimethylpentane	0.6737	203	208	234	

[a] Values from ref 18.

managed while still maintaining a linear dependence of U on V. The equilibration time for each volume was 250 ps, and the data collection times were 500 ps. The resulting plots of internal energy vs volume are shown in Figure 3 for the C7 series and in Figure 4 for the C30 series. The slopes of these plots are the simulation internal pressure (see eq 5).

Results and Discussion

The C7 Series. The experimental density, cohesive energy density, and internal pressure for the C7 series, obtained as described elsewhere,[18] are given in Table 4, which contains the results from simulation as well. The relationship between experimental and simulation values of the cohesive energy density for C7 materials is shown in Figure 5. The line is drawn through the origin with unit slope; it indicates a slight tendency of the simulations to overestimate Π_{CED}, but overall the

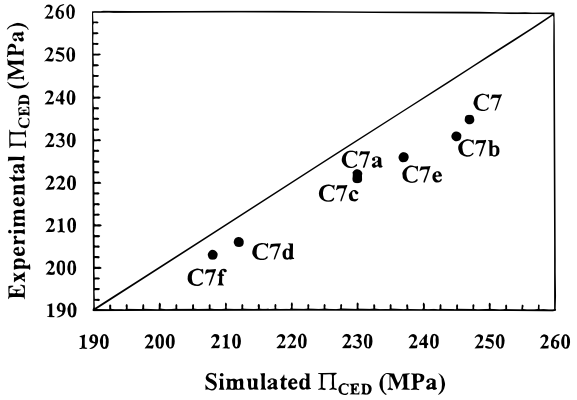

Figure 5. Comparison of experimental and simulated cohesive energy density for the C7 series. The line corresponds to $(\Pi_{CED})_{exp} = (\Pi_{CED})_{sim}$.

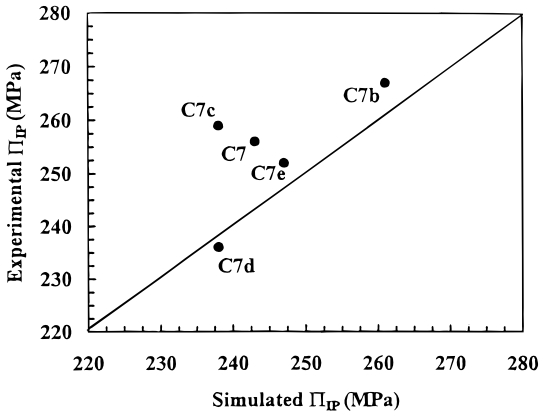

Figure 6. Comparison of experimental and simulated internal pressure for the C7 series. The line corresponds to $(\Pi_{IP})_{exp} = (\Pi_{IP})_{sim}$.

agreement is excellent. The differences between simulation and experiment are only about 5%, not much larger than the uncertainty of the experimental values themselves.

As seen in Figure 6, the correspondence between experiment and simulation is less clear-cut for the internal pressure than that for the cohesive energy density. The major trends are captured, but the departures from the trend line are at least doubled. Some of the increased scatter probably arises from the greater uncertainty in evaluating internal pressure. Thus, both $(\Pi_{CED})_{sim}$ and $(\Pi_{CED})_{exp}$ are essentially single-point properties, but $(\Pi_{IP})_{sim}$ and $(\Pi_{IP})_{exp}$ are derivative quantities, obtained from the slope of U vs V in the simulations and from measurements of isothermal compressibility and thermal expansion coefficient in the experiments.[1,18]

The C30 Series. The simulation values of cohesive energy density and internal pressure for the C30 series at 150 °C are given in Table 5. That table also contains the experimental internal pressures for the corresponding polymeric species at 167 °C. The relationship between $(\Pi_{IP})_{sim}$ and $(\Pi_{IP})_{exp}$ is shown in Figure 7. The solid line corresponds to $(\Pi_{IP})_{exp} = (\Pi_{IP})_{sim}$, so the experimental values of Π_{IP} are generally larger. However, aside from the PIB result, the trend with species is clearer than that found for the C7 series (Figure 6).

The relationship between simulation values of cohesive energy density and internal pressure is shown in Figure 8. All values lie below the $\Pi_{CED} = \Pi_{IP}$ line, so Π_{CED} is smaller than Π_{IP} for all species. Again, PIB is

Table 5. Cohesive Energy Density and Internal Pressure at 150 °C for the C30 and Polymeric Species

	Π_{CED} (MPa)		Π_{IP} (MPa)		
structure	C30 simul	polymeric simul	C30 simul	polymeric simul	polymeric exptl[a]
PE	232	257	274	334	312
hhPP	198	209	243	281	278
iPP	174	178	219	237	252
aPP	178				252
sPP	183				
PB	184		227		245
PEP	207		255		280
PEB	210		261		278
PIB	183		207		302

[a] Values at 167 °C from ref 1.

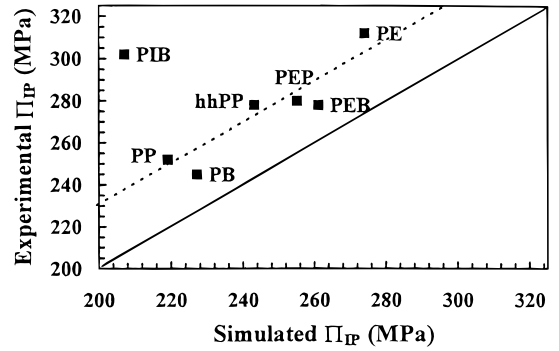

Figure 7. Comparison of experimental and simulated internal pressure for the C30 series. The solid line corresponds to $(\Pi_{IP})_{exp} = (\Pi_{IP})_{sim}$; the dashed line is a guide to the eye.

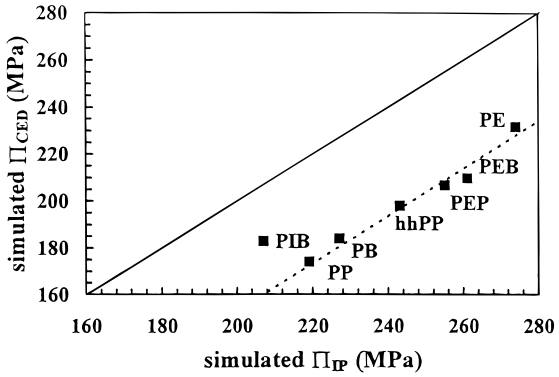

Figure 8. Comparison of simulated cohesive energy density and simulated internal pressure for the C30 series. The solid line corresponds to $\Pi_{CED} = \Pi_{IP}$; the dashed line is a guide to the eye.

exceptional, but the trend for the other six species is now very clear. The anomalous behavior of PIB may be the result of imperfections in the modeling of its united atom potentials; further refinement will be necessary before a definite conclusion on that point can be reached. However, PIB is unique among saturated hydrocarbon polymers in many of its properties,[27] so the departures here may be just one more such example.

Among the C30 properties listed in Table 5 are simulation values of cohesive energy density and internal pressure for isotactic, atactic, and syndiotactic polypropylene (iPP, aPP, and sPP). From these results, the effects of tacticity would appear to be rather slight. Thus, Π_{CED} increases steadily from isotactic to atactic to syndiotactic, but the total variation from isotactic to syndiotactic is only about 5%. These results are consistent with experimental values,[1,28] $(\Pi_{IP})_{aPP}/(\Pi_{IP})_{iPP} =$ 1.0 and $(\Pi_{IP})_{sPP}/(\Pi_{IP})_{iPP} = 1.07$, but are in conflict with a recent PRISM estimate,[28] which suggests $(\Pi_{CED})_{sPP}/(\Pi_{CED})_{iPP} = 1.39$. However, PRISM results are dependent on the single-chain structure factor used as input. In this particular case, the characteristic ratios for sPP and iPP were widely separated, indicating more efficient packing for sPP and resulting in its higher cohesive energy density. Cohesive energy densities were also determined for the same three tacticities of hhPP. The differences, ±1 MPa, were even smaller than those found for PP.

Table 6. Values of Π_{CED}/Π_{IP} from Simulation for C7, C30, and Polymeric Species

structure		Π_{CED}/Π_{IP}		
C7	C30, polymer	C7	C30	polymer
n-heptane	PE	1.02 (0.92)[a]	0.85	0.77
2,3-dimethylpentane	hhPP	0.97 (0.86)	0.82	0.74
2,4-dimethylpentane	iPP	0.89 (0.87)	0.79	0.75
3-methylhexane	PEP	0.96 (0.90)	0.81	
3-ethylpentane	PEB	0.94 (0.87)	0.80	
	PB		0.81	
	PIB		0.88	

[a] Ratios in parentheses are based on the experimental values (Table 4).

The simulation values of cohesive energy density for the C30 series cannot be compared directly with experiment, but data for some of the polymeric versions have been obtained with the PRISM model.[29] Numerically, Π_{CED} from simulation and PRISM differ (257 and 234 MPa, respectively, for PE at 150 °C), but their ordering of values according to species is the same. Thus, $(\Pi_{CED})_{PEP}/(\Pi_{CED})_{PE}$, $(\Pi_{CED})_{PIB}/(\Pi_{CED})_{PE}$, and $(\Pi_{CED})_{iPP}/(\Pi_{CED})_{PE}$ are 0.92, 0.83, and 0.72 from the simulations and 0.91, 0.82, and 0.77 from PRISM.

Extrapolation to Polymeric Values. An examination of the C7 and C30 simulations suggests that the ratio of cohesive energy density to internal pressure, Π_{CED}/Π_{IP}, changes with increasing chain length, varying from approximately unity for the C7 series to somewhat smaller values for C30 materials. The main interest here is in polymeric values of Π_{CED} and Π_{IP}, so, given the rapid rise in computation time with increasing chain length, investigation of the polymeric range requires some scheme of extrapolation. Cohesive energy density and internal pressure were evaluated at various chain lengths for PE (N = 12, 20, 30, 44, and 66 united atoms), hhPP (N = 13, 24, 31, and 41 united atoms), and iPP (N = 13, 22, 31, and 40 united atoms). The results are plotted as functions of reciprocal chain length in Figure 9. The values of both Π_{CED} and Π_{IP} rise with increasing chain length, and those for Π_{IP} rise more rapidly, with the result that the ratio Π_{CED}/Π_{IP} decreases with increasing chain length. A linear relationship with N^{-1} describes the Π_{CED} and Π_{IP} data reasonably well. The polymeric values, obtained by extrapolation to $N^{-1} = 0$, are listed with the C30 results in Table 5. Considering both model and experimental uncertainties, the agreement for all three species between the polymeric values of $(\Pi_{IP})_{sim}$ and $(\Pi_{IP})_{exp}$ is good.

The $\Pi_{CED}-\Pi_{IP}$ Relationship. The values of Π_{CED}/Π_{IP} from C7, C30, and polymeric results are listed in Table 6. As commented earlier, there is a downward trend with increasing chain length, and, for the three polymeric values obtained, the ratios are virtually the same:

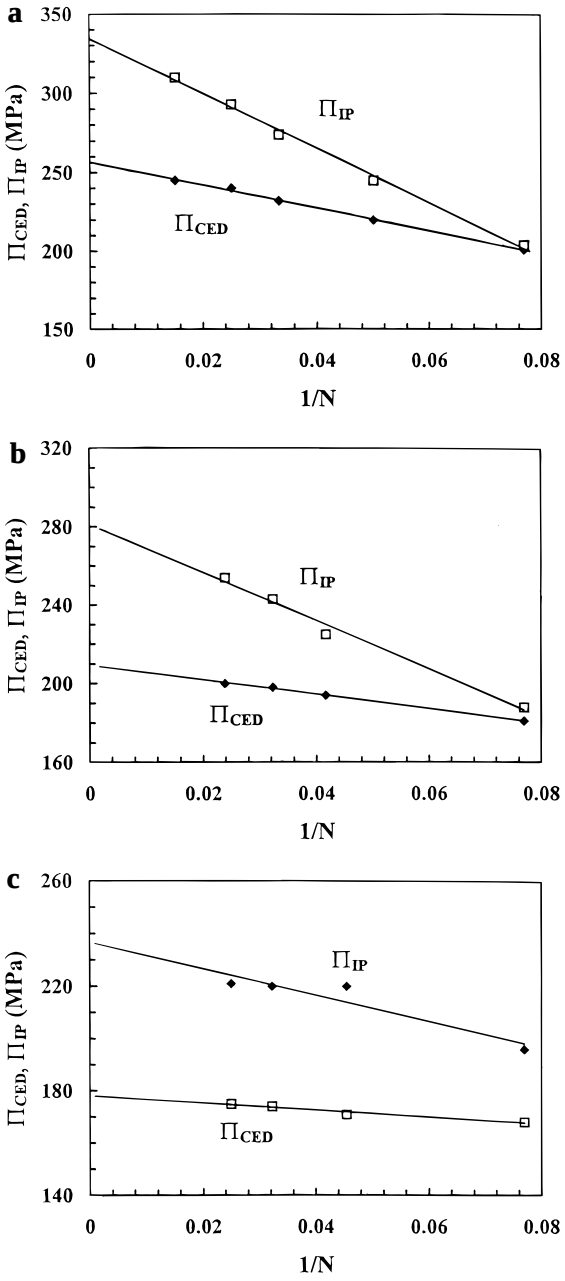

Figure 9. Chain length dependence of cohesive energy density and internal pressure for PE (a), hhPP (b), and iPP (c).

$$\left(\frac{\Pi_{CED}}{\Pi_{IP}}\right)_{sim} = 0.75 \pm 0.02 \qquad (11)$$

Such near equality of Π_{CED}/Π_{IP} values among the three species is perhaps coincidental. The average for this admittedly small set of data does, however, fall in the range of values suggested by the interaction coefficients for polyolefin blends that mix regularly. Thus, a correlation had been established[1] between relative solubility parameters inferred from the interactions, $(\delta - \delta_{ref})_{SANS}$, and those deduced by applying eq 3 to internal pressure data, $(\delta - \delta_{ref})_{PVT}$. From eq 14 of ref 1 and at 167 °C, where data for the most species were available,

$$(\delta - \delta_{ref})_{PVT} = [1.18 \pm 0.09](\delta - \delta_{ref})_{SANS} \qquad (12)$$

Suppose the solubility parameters inferred from the interactions truly originate from cohesive energy density. Then, from eq 3, $(\Pi_{IP}/\Pi_{CED})^{1/2} = (\delta - \delta_{ref})_{PVT}/(\delta - \delta_{ref})_{SANS}$, and, from eq 12,

$$\left(\frac{\Pi_{CED}}{\Pi_{IP}}\right)_{exp} = 0.72 \pm 0.11 \qquad (13)$$

Equation 11 is based on simulations in which only energy was calculated. Equation 13 is derived from experimental data on blend interactions. The agreement between eqs 11 and 13 thus carries the strong implication that the effects governing phase behavior in polyolefin blends with regular mixing are primarily enthalpic in nature. Accordingly, noncombinatorial entropy effects[5,6] and other sources of significant entropic contributions[13−15] would appear to be relatively unimportant in polyolefin blends that mix regularly. The results found here are thus in agreement with PRISM findings[11] and inferences drawn from the experimental data,[4] that these energetic effects are strongly and directly linked to differences in the local chain architecture and packing.

Concluding Remarks

The simulations reported here lend support at the microscopic level to the idea that the interactions governing phase behavior in mixtures of saturated hydrocarbon polymers are primarily enthalpic in nature and linked to differences in local packing. Further, they are consistent with the solubility parameter formulation[3] in that $(\delta - \delta_{ref})_{SANS}$, inferred from the regular mixing behavior of a component, and $(\delta - \delta_{ref})_{CED}$, deduced from its intermolecular energy alone, are essentially identical properties. As commented earlier, a large fraction of the saturated hydrocarbon polymer pairs studied were found to mix regularly. That group would appear to constitute the only extensive collection of liquid pairings, small-molecule or polymeric, whose mixing behavior conforms quantitatively to solubility parameter theory. The simulation results are still quite limited in extent, so, of course, these conclusions should be considered tentative until more data are obtained.

Finally, we wish to comment briefly upon the observation that Π_{IP} is significantly larger than Π_{CED} in the polymeric range. Equality of Π_{CED} and Π_{IP} is a general property of the van der Waals model for the dense liquid state,[3] and, as noted here and elsewhere,[3,18] equality is, indeed, a good approximation for liquids of small nonpolar molecules. In the van der Waals model, the molecules are treated as spheres, and hence the pair distribution function is entirely intermolecular: $[g(r)]_{inter} = [g(r)]_{total}$. For chain molecules, $[g(r)]_{intra}$ must also be considered, and $[g(r)]_{inter}$ and $[g(r)]_{intra}$ evolve with increasing chain length to approach eventually their species-dependent polymeric forms. We suggest that the variation of Π_{CED}/Π_{IP} with chain length is related to this evolution of $[g(r)]_{inter}$ and $[g(r)]_{intra}$. We assume that Π_{CED} depends only on $[g(r)]_{inter}$, and, indeed, the simulation values of Π_{CED} were calculated in that way. We speculate, however, that Π_{IP} is more closely linked with $[g(r)]_{total}$. Thus, for organic liquids at ambient pressures, and with thermodynamic identities alone, eq 5 can be written[3]

$$\Pi_{IP} = T\left(\frac{\partial P}{\partial T}\right)_v \qquad (14)$$

in which $(\partial P/\partial T)_v$ is the thermal pressure coefficient γ. Being a mechanical property, γ depends primarily on how each chain unit interacts with all neighboring units, whether they belong to its own chain or some other. Accordingly, Π_{IP} reflects $[g(r)]_{total}$ and, to that extent, should be larger than Π_{CED} in the long-chain limit. As with the other tentative conclusions in the paper, simulations extrapolated to the polymeric limit for many more species would be useful for testing generality.

Acknowledgment. Funding for this work was provided by the National Science Foundation through Grants CTS97-04907 and DMR98-04327 (S.K.K.) and DMR93-10762 (W.W.G.), and by the Department of Energy through Grant DE-FG02-87ER13714 (P.G.D.). We are grateful to Dr. Mark Disko of Exxon Corporate Laboratories for discussions about alternative simulation models. We are also grateful to K. S. Schweizer for his valuable comments on the manuscript.

References and Notes

(1) Krishnamoorti, R.; Graessley, W. W.; Dee, G. T.; Walsh, D. J.; Fetters, L. J.; Lohse, D. J. *Macromolecules* **1996**, *29*, 367.
(2) Reichart, C. G.; Graessley, W. W.; Register, R. A.; Krishnamoorti, R.; Lohse, D. J. *Macromolecules* **1997**, *30*, 3036.
(3) Hildebrand, J. H.; Scott, R. L. *The Solubility of Nonelectrolytes*; Dover Pulications: New York, 1964.
(4) Graessley, W. W.; Krishnamoorti, R.; Reichart, G. C.; Balsara, N. P.; Fetters, L. J.; Lohse, D. J. *Macromolecules* **1995**, *28*, 1260.
(5) Bates, F. S.; Schultz, J. H.; Rosedale, J. H.; Almdal, K. *Macromolecules* **1992**, *25*, 5547.
(6) Fredrickson, G. H.; Liu, A. J.; Bates, F. S. *Macromolecules* **1994**, *27*, 2503.
(7) Weinhold, J. D.; Kumar, S. K.; Singh, C.; Schweizer, K. S. *J. Chem. Phys.* **1995**, *103*, 9460.
(8) Singh, C.; Schweizer, K. S. *J. Chem. Phys.* **1995**, *103*, 5418.
(9) Schweizer, K. S. *Macromolecules* **1993**, *26*, 6050.
(10) Singh, C.; Schweizer, K. S. *Macromolecules* **1995**, *28*, 8692.
(11) Schweizer, K. S.; Singh, C. *Macromolecules* **1995**, *28*, 2063.
(12) Singh, C.; Schweizer, K. S. *Macromolecules* **1997**, *30*, 1490.
(13) Freed, K. F.; Dudowicz, J. *Macromolecules* **1996**, *29*, 625. Dudowicz, J.; Freed, K. F. *Macromolecules* **1996**, *29*, 8960; **1997**, *30*, 5506.
(14) Foreman, K. W.; Freed, K. F. *J. Chem. Phys.* **1997**, *106*, 7422; *Macromolecules* **1997**, *30*, 7279.
(15) Freed, K. F.; Dudowicz, J.; Foreman, K. W. *J. Chem. Phys.* **1998**, *108*, 7881.
(16) Maranas, J. K.; Kumar, S. K.; Debenedetti, P. G.; Graessley, W. W.; Mondello, M.; Grest, G. S. *Macromolecules* **1998**, *31*, 6998.
(17) Krishnamoorti, R.; Graessley, W. W.; Balsara, N. P.; Lohse, D. J. *Macromolecules* **1994**, *27*, 3073.
(18) Allen, G.; Gee, G.; Wilson, G. J. *Polymer* **1960**, *1*, 456.
(19) Jorgensen, W. L.; Madura, J. D.; Swenson, C. J. *J. Am. Chem. Soc.* **1984**, *106*, 6638.
(20) Boyd, R. H.; Krishna Pant, P. V. *Macromolecules* **1991**, *24*, 6325.
(21) Krishna Pant, P. V.; Boyd, R. H. *Macromolecules* **1993**, *26*, 679.
(22) Maranas, J. K. Ph.D. Thesis, Princeton University 1997.
(23) Doolittle, A. K. *J. Chem. Eng. Data* **1964**, *9*, 275.
(24) Berendsen, H. J. C.; Postma, J. P. M.; Van Gunsteren, W. F.; Di Nola, A.; Haak, J. R. *J. Chem. Phys.* **1984**, *81*, 3684.
(25) Allen, M.; Tildesley, D. *Computer Simulation of Liquids*; Clarendon Press: Oxford, 1976.
(26) Hansen, J. P.; McDonald, I. R. *The Theory of Simple Liquids*, 2nd ed.; Academic Press: Orlando, FL, 1986.
(27) Krishnamoorti, R.; Graessley, W. W.; Fetters, L. J.; Garner, R. T.; Lohse, D. J. *Macromolecules* **1995**, *28*, 1252.
(28) Maier, R.-D.; Thomann, R.; Kressler, J.; Mülhauptt, R.; Rudolf, B. *J. Polym. Sci.: Phys.* **1997**, *35*, 1135.
(29) Schweizer, K. S.; David, E. F.; Singh, C.; Curro, J. G.; Rajasekaran, J. J. *Macromolecules* **1995**, *28*, 1528.

MA9717552